Comparison of the Beta Spectra of B^{12} and N^{12}†

T. MAYER-KUCKUK* AND F. C. MICHEL
California Institute of Technology, Pasadena, California
(Received March 12, 1962)

The conserved-vector-current (CVC) theory predicts a deviation from the allowed shape of the B^{12} and N^{12} beta spectra. The ratio of the shape factors of the two spectra is expected to have an energy dependence of $(1.10\pm0.17)\%$ per MeV. If the CVC hypothesis is not invoked, this ratio is estimated to be an order of magnitude smaller. The two spectra have been measured with a magnetic spectrometer and found to give for this ratio the value $(1.30\pm0.31)\%$ per MeV. The branching fraction of the N^{12} decay to the 7.6-MeV state of C^{12} has been determined to be $(3.0\pm0.5)\%$.

I. INTRODUCTION

THE observed near-equality of the vector beta-decay coupling constant given by the decay of O^{14} and the muon-decay coupling constant led Feynman and Gell-Mann[1] to postulate the conservation of the vector part of the beta-decay current. Gell-Mann[2] pointed out that, as a consequence of this conserved-vector-current (CVC) theory, an appreciable and calculable term is added to the beta-decay interaction. The appearance of this term is analogous to the situation in electromagnetism where, in order to describe the interaction, it is necessary to add to the Dirac Hamiltonian a term representing the additional interaction with the anomalous magnetic moments. As a test of this prediction, Gell-Mann[2] suggested a comparison of the beta-decay spectra of B^{12} and N^{12}.

Some considerable support for the hypothesis of a conserved vector current has already appeared in experiments on beta decay. In the decay $F^{20}(\beta^-)Ne^{20*}(\gamma)Ne^{20}$, Boehm, Soergel, and Stech[3] found a beta-gamma angular correlation with sign and magnitude consistent with estimates from the CVC theory. A more quantitative test is provided by the beta-alpha correlation in the mirror decays $Li^8(\beta^-)Be^{8*}(\alpha)He^4$ and $B^8(\beta^+)Be^{8*}(\alpha)He^4$ reported by Nordberg, Morinigo, and Barnes,[4] where agreement was found within limits imposed by a shell-model calculation of the relevant $M1$ matrix element. Precise measurements of the O^{14} decay energy and half-life[5] have established that the beta-decay and muon-decay coupling constants differ by only about 1.8%, with an uncertainty which depends largely on theoretical corrections. The present report concerns a direct comparison between the spectra of B^{12} and N^{12} where some of the uncertainties which have attended the previous work can be avoided. A short account of this work has been published earlier[6]; the more detailed analysis presented here has led to a slightly different numerical result, but to no change in the conclusion.

Figure 1 exhibits the principal features of the decay schemes[7] of B^{12} and N^{12}. Boron[12], which has a half-life of 20.3 msec, decays mainly (97%) to the ground state of C^{12} with a maximum electron energy of 13.369 MeV. Nitrogen[12], with a half-life of 11.4 msec, also decays mainly to the ground state of C^{12}, with a maximum positron energy of 16.43 MeV. The two radionuclides are members of a $T=1$ triplet, whose central member is the 15.11-MeV level of C^{12}. The ground states of B^{12} and N^{12} are $J^\pi=1^+$, while the C^{12} ground state is 0^+.

In beta transitions of the character $J^\pi=1^+\rightarrow0^+$, $\Delta T=1$, only the allowed and second-forbidden axial vector and second-forbidden vector-matrix elements contribute. The second-forbidden vector term gives rise

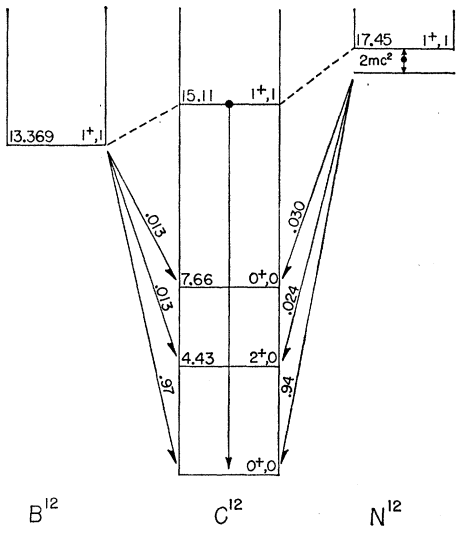

FIG. 1. Energy-level diagram of the triad B^{12}, C^{12}, and N^{12}. Only the transitions and levels of importance for this paper are indicated. The notation is standard.

† Supported in part by the Joint Program of the Office of Naval Research and the U. S. Atomic Energy Commission.
* Now at the Max Planck Institut für Kernphysik, Heidelberg, Germany.
[1] R. P. Feynman and M. Gell-Mann, Phys. Rev. **109**, 193 (1958); see also earlier work by S. S. Gershtein and J. B. Zeldovich, Zhur. Eksptl. i Teoret. Fiz. **29**, 698 (1955) [translation: Soviet Phys.—JETP **2**, 576 (1957)].
[2] M. Gell-Mann, Phys. Rev. **111**, 362 (1958).
[3] F. Boehm, V. Soergel, and B. Stech, Phys. Rev. Letters **1**, 77 (1958).
[4] M. E. Nordberg, Jr., F. B. Morinigo, and C. A. Barnes, Phys. Rev. Letters **5**, 321 (1960); and Phys. Rev. **125**, 321 (1962).
[5] R. K. Bardin, C. A. Barnes, W. A. Fowler, and P. A. Seeger, Phys. Rev. Letters **5**, 323 (1960); and (to be published).
[6] T. Mayer-Kuckuk and F. C. Michel, Phys. Rev. Letters **7**, 167 (1961).
[7] F. Ajzenberg-Selove and T. Lauritsen, Nuclear Phys. **11**, 1 (1959).

to an energy dependence of the transition-matrix element of the form

$$|M|^2=\text{const}(1\pm\tfrac{1}{2}AE)$$

where E is the beta-particle energy and $\frac{1}{2}A$ is proportional to the interference term between the second-forbidden vector and allowed axial vector-matrix elements. The plus sign applies to electron decay and the minus sign to positron decay. The interference term between the allowed and second-forbidden axial vector-matrix elements is insensitive[2] to E and does not differ in sign between electron and positron decay. The ratio of the transition-matrix elements of the B^{12} decay to the N^{12} decay then becomes, to first order in E,

$$|M(B^{12})|^2/|M(N^{12})|^2=\text{const}(1+AE).$$

The quantity A is analogous to the magnetic dipole transition-matrix element in electromagnetism. In the CVC theory, this analogy becomes exact, and A is given by a combination of known constants times the transition value of the magnetic moment operator $\mathfrak{y}$. From electromagnetism we have, aside from a constant factor,

$$\mathfrak{y}=[(1+\mu^s)+(1+\mu^v)\tau_z]\boldsymbol{\sigma}+[1+\tau_z]\mathbf{l},$$

where $\mu^s=-0.12$ and $\mu^v=3.70$ are the isotopic scalar and vector nucleon anomalous magnetic moments in isotopic spin formalism. For a $\Delta T=1$ transition, only the isotopic vector terms contribute, and we need only

$$\mathfrak{y}=(1+\mu^v)\boldsymbol{\sigma}\tau_z+\mathbf{l}\tau_z.$$

In the Fermi[8] theory the same relation holds between A and $\mathfrak{y}$ except that μ^v (beta decay) will not necessarily have the same value as μ^v(electromagnetic). If the pion current contribution to the electromagnetic interaction of the nucleon were omitted, then μ^v (electromagnetic) would essentially vanish. Gell-Mann[9] gives, analogously, μ^v (beta decay)≈ 0 as a reasonable guess for the Fermi theory. A dispersion theoretic treatment by Goldberger and Treiman[10,11] verifies this in estimating $\mu^v(\text{F})\approx(1/15)\mu^v$ (CVC). We then have

$$A(\text{CVC})=K\langle\|4.70\boldsymbol{\sigma}\boldsymbol{\tau}+\mathbf{l}\boldsymbol{\tau}\|\rangle$$
$$A(\text{F})\quad\approx K\langle\|1.25\boldsymbol{\sigma}\boldsymbol{\tau}+\mathbf{l}\boldsymbol{\tau}\|\rangle$$

If $\langle\|\mathbf{l}\boldsymbol{\tau}\|\rangle/\langle\|\boldsymbol{\sigma}\boldsymbol{\tau}\|\rangle$ is large, then measuring A is not a sensitive test; however an intermediate coupling analysis[12] of the transition under consideration indicates that this ratio is small (less than 0.1).

The value of 4.70 is appropriate for a free nucleon; thus to improve the estimate of A, the transition-matrix element $\langle\|\mathfrak{y}\|\rangle$ is determined from the gamma-decay width of the 15.11-MeV state of C^{12}, the $T_z=0$ analog of the ground states of B^{12} and N^{12}. The value of A is then computed[2,9] to be

$$A(\text{CVC})=(1.33\pm0.15)\%\text{ per MeV.}$$
$$A(\text{F})\quad\approx 0.35\qquad\%\text{ per MeV.}$$

The uncertainty in A comes mainly from the uncertainty in the C^{12} gamma-decay (15.11 MeV) rate, where the experimental value $\Gamma_\gamma=53\pm11$ eV, derived from the work of Hayward and Fuller[13] has been used. Taking into account the more recent determinations of Garwin[14] ($\Gamma_\gamma=59.2\pm9.7$ eV), Barber *et al.*[15] ($\Gamma_\gamma=40\pm7$ eV), and Hanna and Segel[16] ($\Gamma_\gamma=50.5\pm7.1$ eV) yields a weighted average value $\Gamma_\gamma=50\pm4$ eV and $A=1.29\pm0.07\%$ per MeV. Taking into account the 20% larger ft value of N^{12} increases this by 5% to 1.35 ± 0.07. No attempt has been made to assess the uncertainty in the value of A estimated from the Fermi theory.

In deriving the ratio of matrix elements from the observed spectra, it is necessary to make corrections for components arising from transitions to excited states of C^{12}, and, in addition, corrections for inner bremsstrahlung and other electromagnetic effects. The last have been computed by Gell-Mann and Berman[9] who give an expression of the form

$$S(E,B^{12})/S(E,N^{12})=\text{const}[1+(A+\delta A)E]f(E),$$

where $S(E)$ is the experimental spectrum, corrected for branching to excited states of C^{12}, and divided by the appropriate Fermi spectrum. The electromagnetic corrections are represented by δA, estimated to be $-0.25\pm0.15\%$ per MeV, while the quantity $f(E)$ represents the ratio, $f(E,B^{12})/f(E,N^{12})$, of the inner bremsstrahlung corrections[17] to the spectra of B^{12} and N^{12}. With this correction assumed calculable in the range needed, the experiment determines $(A+\delta A)$, which is to be compared with the predicted values,

$$A+\delta A=(1.10\pm0.17)\%\text{ per MeV (CVC)}$$
$$\approx 0.10\qquad\%\text{ per MeV (F)}$$

II. APPARATUS

The beta spectra of B^{12} and N^{12} were analyzed with an iron-free single-lens magnetic spectrometer directly connected to a 3-MeV van de Graaff accelerator. The B^{12} was produced in the reaction $B^{11}(d,p)B^{12}$, and N^{12} was produced in the reaction $B^{10}(He^3,n)N^{12}$. The targets were located at the object point of the spectrometer. The deuteron or He^3 beam was periodically interrupted at a frequency of 60 cps and the beta particles counted in an anthracene scintillator after suitable delay. The

[8] The theory of beta decay without invoking the CVC hypothesis is referred to here as the "Fermi" theory.
[9] M. Gell-Mann and S. M. Berman, Phys. Rev. Letters **3**, 99 (1959).
[10] M. L. Goldberger and S. B. Treiman, Phys. Rev. **111**, 354 (1958).
[11] M. L. Goldberger, Revs. Modern Phys. **31**, 797 (1959).
[12] H. A. Weidenmüller, Nuclear Phys. **21**, 397 (1960).
[13] E. Hayward and E. G. Fuller, Phys. Rev. **106**, 991 (1957).
[14] E. L. Garwin, Phys. Rev. **114**, 143 (1959).
[15] W. C. Barber, F. Berthold, G. Fricke, and F. E. Gudden, Phys. Rev. **120**, 2081 (1960).
[16] S. S. Hanna and R. E. Segel, Proc. Roy. Soc. (London) **A259**, 267 (1960).
[17] T. Kinoshita and A. Sirlin, Phys. Rev. **113**, 1652 (1959).

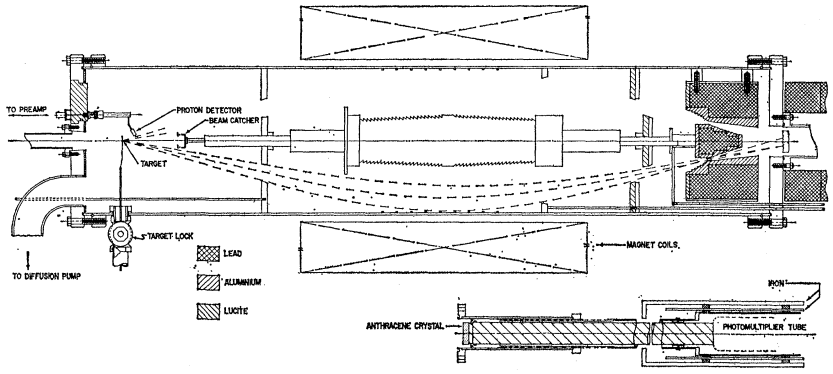

FIG. 2. The spectrometer in cross-sectional view with the axis of symmetry along the beam direction. The magnet coils are not shown full diameter. Dotted lines indicate the electron trajectories for the extreme and mean acceptance angles. Unless otherwise indicated, the material is brass.

production rate of the activity was monitored by the reaction protons from $B^{10}(d,p)B^{11}$ for B^{12} and $B^{10}(He,p)C^{12}$ for N^{12}. A silicon p-n junction counter served as a proton detector.

Spectrometer

The spectrometer used here is essentially that described by Hornyak *et al.*,[18] except that the baffle system was modified for the high beta-particle energies involved. This arrangement is illustrated in Fig. 2. As can be seen in this figure, the baffles on the counter end of spectrometer were all faced with lucite. The lucite was coated with a conducting layer of carbon to inhibit static charging. To further reduce scattering, the walls of the spectrometer were lined with narrow brass rings to serve as traps for forward-scattered electrons. Similarly, the central brass absorber was machined to have the saw-toothed cross section shown in the figure. The ring focus slits were of aluminum, so shaped as to permit the minimum possible transmission of particles outside the selected momentum range. The spectrometer was aligned using a special baffle and counter arrangement to define the electron trajectories.[19] The best source and counter position could be determined to within 0.3 mm. The final experimental arrangement was quite insensitive to such small displacements. With a calibrated Bi^{207} source, the transmission was experimentally determined to be 0.85% and the resolution to be 1.5%. Energy calibration was accomplished using the conversion lines of Cs^{137}, Bi^{207}, and thorium deposit. The least-squares fit to these points gave an uncertainty of 4×10^{-4} in the magnetic rigidity $B\rho$ for a given current setting. The earth's magnetic field was reduced to less than 1/10 of its ambient value in each axis of the spectrometer by using three orthogonal sets of compensating coils.

Beta Detector

The beta-particle detector consisted of a 10-mm thick, 38-mm diameter anthracene crystal mounted on a 90-cm long lucite light pipe leading to an RCA 6292 photomultiplier tube. The tube was shielded from the stray magnetic field of the spectrometer by three mu-metal layers wrapped directly on the photomultiplier tube and two concentric cylinders of soft iron. An 0.5 mg/cm^2 aluminum window covered the crystal. The effect of the magnetic field on the photomultiplier was checked using a Po^{210} source and a thin CsI crystal. The line shift was less than one percent in energy between zero and the maximum field used in this experiment. No change in shape or area of the pulse-height distribution was observed.

The pulse-height distributions recorded on a 100-channel analyzer for two ranges of beta-particle energies are displayed in Figs. 3 and 4. It may be observed in Fig. 4 that the high-energy electrons give nearly identical pulse-height distributions for energies above 5 MeV. The "double-peaked" distributions at the lower energies are discussed by Porter *et al.*[20] The lower energy peak is ascribed to electrons that pass through the crystal, while the second peak represents electrons that are scattered through large angles within the crystal and hence stop in the crystal. Below 2.3 MeV, the energy of electrons having a range equal to the crystal thickness, all of the electrons stop in the crystal and hence the two peaks merge into a single peak. At very high energies it is un-

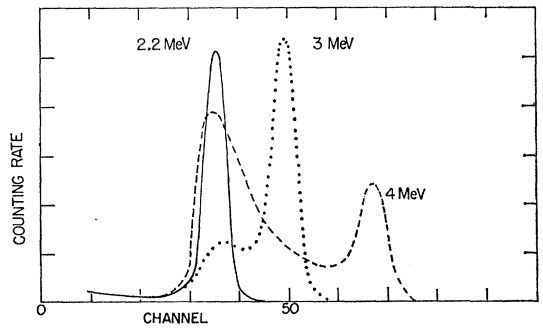

FIG. 3. Pulse-height distributions in the thin anthracene crystal for low-energy beta particles from B^{12}.

[18] W. F. Hornyak, T. Lauritsen, and V. K. Rasmussen, Phys. Rev. **76**, 731 (1949).

[19] V. K. Rasmussen, Ph.D. thesis, California Institute of Technology, 1950 (unpublished).

[20] F. T. Porter, M. S. Freedman, T. B. Novey, and F. Wagner, Jr., Phys. Rev. **103**, 921 (1956).

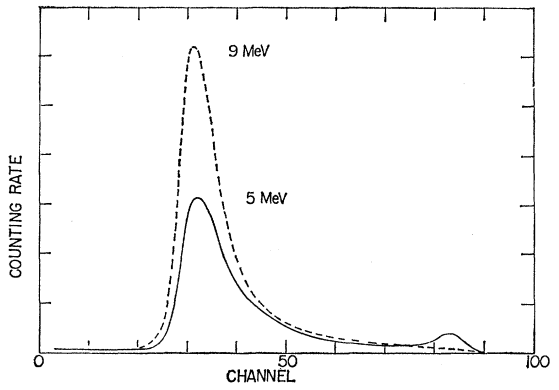

FIG. 4. Pulse-height distributions in the thin anthracene crystal for high-energy beta particles from B^{12}.

likely that an electron will stop in the crystal and one again observes only a single peak.

The pulse-height distributions were continuously monitored during the actual runs, and the total count was recorder by a scaler which counted all pulses above a given channel. Figures 5 and 6 are experimental pulse-height distributions of 8-MeV beta particles from B^{12} and N^{12} including background. The background was separately determined from measurements at zero field and high ($>E_{max}$) field. To estimate the number of real counts below channel 21 in Fig. 5 we assume, from the near constancy of the difference between the background and 8-MeV counts, that this number is reasonably given by the number of real counts in channels 10 to 30. We then find that about 0.6% of the true counts fall below the discriminator level at 8 MeV. The same number is obtained from the observed distribution of 5- and 10.5-MeV B^{12} electrons. Since this quantity does not appear to be energy dependent, no correction is necessary for these counts.

The approximately uniform intensity of small pulses over a large channel spread, as seen in Fig. 5, is significant for another reason. The channel in which a pulse

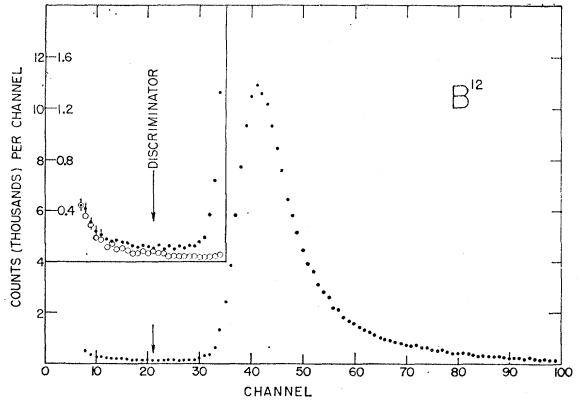

FIG. 5. Pulse-height distributions for 8.0-MeV electrons from B^{12} and background. The insert shows the small pulse tail amplified by a factor of five.

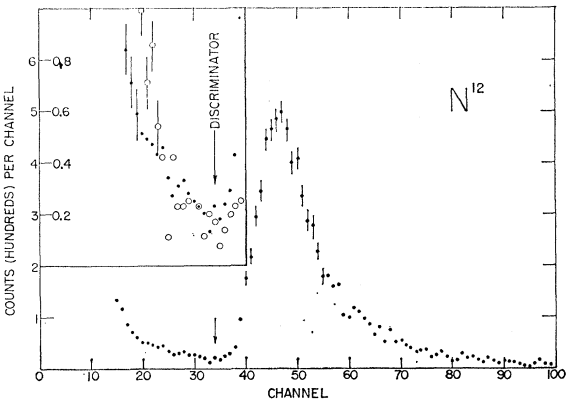

FIG. 6. Pulse-height distributions for 8.0-MeV positrons from N^{12} and background. The insert shows the small pulse tail amplified by a factor of five. The vertical bars indicate $\sqrt{N}$ for several channels where N is the number of counts in that channel.

appears is, for high-energy electrons, directly proportional to the path length of the electron in the crystal. The only part of the pulse-height spectrum inaccessible corresponds then to the very short path lengths. Any backscattered electrons not seen in the tail must either lose enough energy to produce a pulse larger than the tail pulses and thereby be counted, or be scattered within a very shallow depth of the crystal. Only the latter can be lost and need to be examined in more detail. If the intensity in channel 10 is assumed to consist entirely of such backscattered electrons, then an upper limit to the total backscattered intensity *lost* may be calculated[21] from the data to be approximately 0.90% at 5 MeV and 0.96% at 11.5 MeV.

The possibility of using a scintillator thick enough to stop all electrons was also examined experimentally, but rejected on the ground that the increased volume led to greatly increased sensitivity to room background, due largely to x rays from the accelerator, and stray neutrons originating in the target.

Proton Detector

The reaction protons from the target were monitored as a measure of the number of active nuclei produced. Since the gating cycle is fixed and the beam pulse fluctuations average out, the total number of protons divided by the total duration of the run (clock time) is then directly proportional to the average activity. A silicon *p-n* junction counter was used to detect the protons. This counter was located inside the spectrometer near the target as shown in Fig. 2. For the B^{12}-reaction monitor the protons from $B^{10}(d,p)B^{11}$ leading to the ground state ($Q=9.2$ MeV) were detected after absorbing the lower energy protons in 118 mg/cm² of aluminum. For the N^{12}-reaction monitor, the protons from

[21] A. H. Wapstra, G. J. Nijgh, and R. Van Lieshout, *Nuclear Spectroscopy Tables* (North-Holland Publishing Company, Amsterdam, 1959), p. 40.

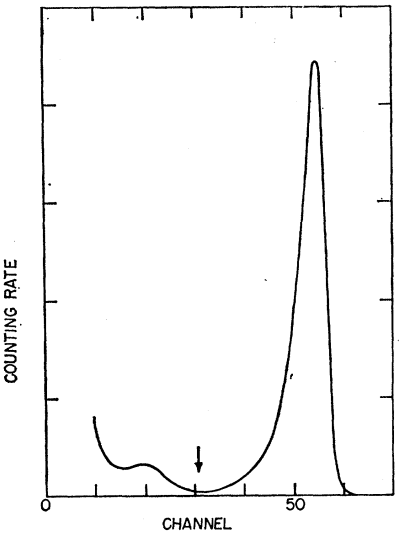

FIG. 7. Pulse-height distribution of protons from $B^{10}(d,p)B^{11}$ in the B^{12} experiment. The protons have passed through 118 mg/cm^2 of aluminum foil before being detected in the p-n junction counter. Arrow indicates the discriminator setting.

$B^{10}(He^3,p)C^{12}$ leading mainly to the first-excited state ($Q=15.3$ MeV) were detected after passing through 344 mg/cm^2 of aluminum. The pulse-height distributions were monitored on a multichannel analyzer. A typical B^{12}-proton spectrum is shown in Fig. 7. No field dependence of the proton spectra could be detected (less than one percent in energy). The solid angle subtended by the proton counter amounted to 0.7% of the sphere.

Circuitry

Figure 8 shows a block diagram of the detection system. The beam is on for 8.3 msec and off for 8.3 msec; the "beam-off" signal triggers the gate generator which, after a delay of 1 msec, turns on the beta-particle scaler for 5.25 msec. The total counting time is monitored by simultaneously counting the oscillations from a 20-kc/sec quartz oscillator. The pulse-height distributions from the beta-particle and proton detectors were monitored and recorded on multichannel analyzers. The "coincidence" scaler checks the operation of the gate generator by recording a count if the beam and beta-particle scaler are on simultaneously. This and the total number of gate pulses were monitored as a check. All the scalers were simultaneously turned on and off by an external timer unit not shown in the figure.

Targets

The targets consisted of approximately 0.3 mg/cm^2 of boron on foils of thickness 0.5 mg/cm^2 and 3 mg/cm^2 for B^{12} and N^{12}, respectively.[22] The boron was deposited on the foils by heating them in a low-pressure atmosphere (less than 15-mm Hg) of diborane gas.[23] This heating was accomplished by focusing the image of an arc light on the foil which was mounted in a frame of 1.5-mil aluminum. For the B^{12} the foils were 5000 Å nickel, and for the N^{12} they were 500 Å nickel on copper backing. This copper backing enabled the target to withstand the strong He^3 beam in the N^{12} experiment, while the boron deposit adhered better to the nickel. Natural boron (19% B^{10}; 81% B^{11}) targets were used for the B^{12} and enriched boron (96% B^{10}; 4% B^{11}) for the N^{12}.

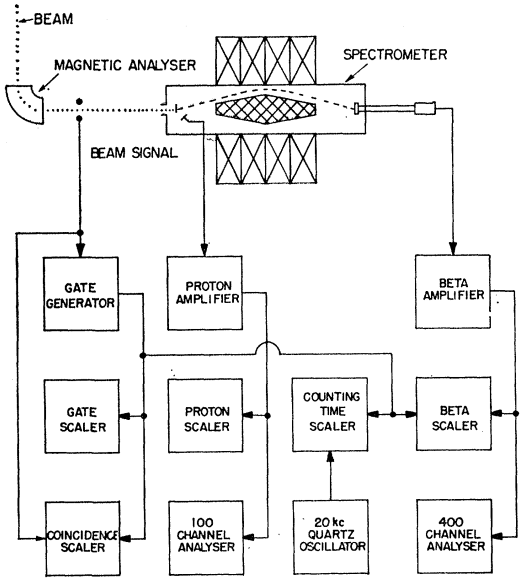

FIG. 8. Block diagram of the counting and gating circuitry.

Bombarding Conditions

The beam from the electrostatic accelerator was magnetically analyzed and brought into the spectrometer to give a beam spot 2-mm square. The size and position of the beam spot were insensitive to changes in the spectrometer field, and it was not necessary to reposition the beam spot for each beta-particle energy. 1.65-MeV deuterons at 0.2 μA were used for the B^{12} and 2.75-MeV He^3 ions at 2–3 μA for the N^{12}. The beam was chopped at the ion source by periodically turning off the rf voltage. The possibility of an HD^+ contamination of the beam, which could produce a B^{12} activity in the N^{12} experiment, was examined by bombarding a natural boron target with a 1.00-MeV He^3 beam. From this experiment it was concluded that less than 8×10^{-4} electrons were produced per positron at the 2.75-MeV bombarding energy on the enriched target.

III. EXPERIMENTAL PROCEDURE AND RESULTS

The spectra were sampled at 0.5-MeV intervals in the range 5–15 MeV for B^{12} and 2.5–18 MeV for N^{12}, the data being collected at alternating high- and low-energy points to minimize effects of target deterioration and instrumental drifts. Each data point consisted of

[22] The B^{12} spectrum was also taken using the thicker 3-mg/cm^2 backing. No influence on the shape factor was found for the energies considered in this paper.

[23] J. Overley, Ph.D. thesis, California Institute of Technology, 1960 (unpublished).

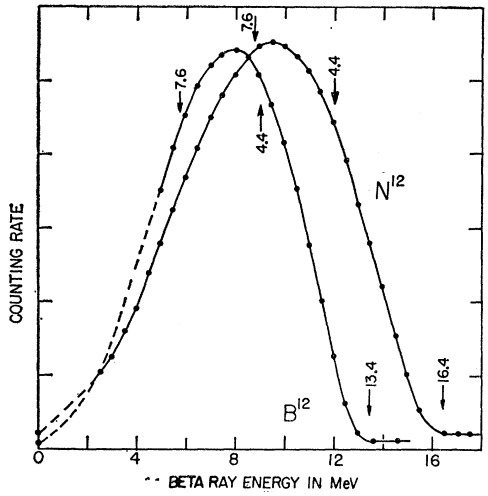

FIG. 9. Counting rate vs energy plot of B^{12} and N^{12} data. Branching end points are indicated by arrows. Background at zero and high field is shown.

the number of beta-particle counts divided by the number of proton counts and by the "live" counting time, determined by the 20-kc/sec oscillator. All points were taken with a fixed total duration (clock time) of 3 min for B^{12} and 10 min for N^{12}.

Figure 9 presents the observed counting rates as a function of energy. These rates have been normalized as indicated above, but have not been corrected for background or adjusted for the variable momentum interval accepted by the spectrometer. Typical counting rates obtained at 8-MeV beta energy were approximately 40 000 electrons/min and 120 000 protons/min for B^{12}, 600 positrons/min and 600 000 protons/min for N^{12}. Typical background corrections at 8 MeV amounted to about 1.7% for B^{12} and 4.2% for N^{12}.

The background was studied at spectrometer settings above the end points of the beta spectra, at zero field, and with blank targets. To simulate the effects of neutrons produced during the bombardment periods, separate studies were made with a beryllium target bombarded by deutrons, examining the background in the normal counting cycle. The counting rate with the beryllium target, which combined the effects of neutrons and general background due to the accelerator, was independent of the spectrometer field setting. In the B^{12} experiment, about one-fourth of the 1.7% background could be accounted for by neutron and general background, and the remainder, about 1.2% at zero field and 1.6% at high field, must be attributed to scattered electrons and/or bremsstrahlung within the spectrometer. The fact that high and zero field were roughly equal suggests the latter as the more plausible. For N^{12} the yield was much smaller and bombarding energies much higher, consequently the neutron and general background were increased by a factor of ten. Thus after subtracting the neutron and general background, about 1.7% remained of the 4.2% N^{12} background. This remaining N^{12} background, about 1.6% at zero field and 1.8% at high field, has a magnitude and variation comparable with the residual B^{12} background which tends to confirm scattering and/or bremsstrahlung as a common background source. In the B^{12} experiment, the variation of the background was studied up to 5 MeV beyond the B^{12} end point and showed little dependence upon the field.

In the spectrum studies, particular attention was given to the regions 5 to 10.5 MeV for B^{12} and 5 to 13 MeV for N^{12}. The lower limit of 5 MeV was dictated by uncertainties introduced by branching to excited states of C^{12}—indicated by arrows on Fig. 9—and the upper limits were held well below the spectrum end points to minimize the effect of uncertainties in calibration and background subtraction. The data for the relevant ranges are exhibited in Table I, in terms of counts per unit momentum interval, corrected for background, as a function of magnetic rigidity. The indicated standard deviations represent combined uncertainties from statistics and background subtraction.

TABLE I. Momentum spectra of B^{12} and N^{12}. Correction for background has been made. Second number indicates combined uncertainty due to background and statistics. The electron momentum is symbolized by η.

$B\rho$(kG-cm)	$N(\eta,B^{12})$	S.D.	$N(\eta,N^{12})$	S.D.
9.898			3649	87
11.587			3903	87
13.270			4631	87
14.950			4980	86
16.628			5748	82
18.302	2898	23	6119	30
19.976	3076	11	6657	31
21.650	3171	10	6998	33
23.323	3212	9	7212	33
24.994	3198	8	7466	35
26.665	3085	7	7503	35
28.336	2933	7	7477	36
30.023	2722	6	7369	36
31.676	2455	6	7215	28
33.346	2139	5	6912	25
35.017	1794	6	6443	29
36.687	1433	6	6066	25
38.355	1061	6	5634	25
40.025	721	6	5021	21
41.696	415	7	4390	19
43.363	183	7	3711	16
45.033	38	5	2998	13
46.704			2413	33
48.373			1804	29
50.042			1158	23
51.711			678	17
53.380			260	14

Results

The measured momentum distributions for B^{12} and N^{12} are tabulated in Table I; the Fermi plots of this data are exhibited in Fig. 10. The end points obtained from this experiment are, for B^{12}, 13.381±0.041 MeV and for N^{12}, 16.36±0.21 MeV, to be compared with values of 13.369±0.001 and 16.43±0.06 MeV, respectively,[24,25] as determined from reaction data.

We first consider the analysis of the B^{12} data. The derivation of the shape factor requires correction for branching to excited states of C^{12}. The end points of these beta-decay branches are known from the level structure of C^{12} and are indicated by arrows in Figs. 9 and 10. The branching fractions to the 4.4 and 7.6-MeV levels have been measured[26–28] to be 1.3±0.1 and

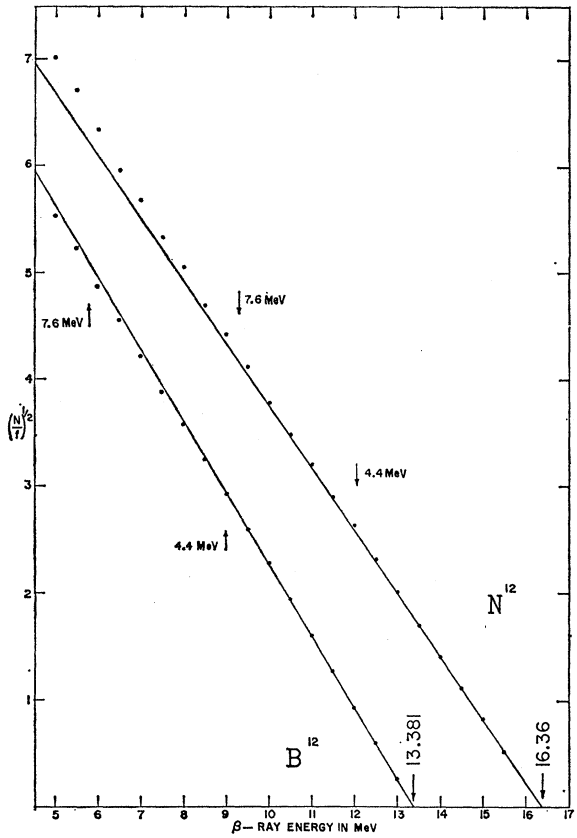

FIG. 10. Fermi plots for B^{12} and N^{12}. The observed end-point energies, indicated in the figure, are in agreement with the values from reaction data of 13.369 MeV for B^{12} and 16.43 for N^{12}. The curvature of the N^{12} plot due to branching can easily be seen. In the B^{12} plot this effect is overcompensated by CVC-shape factors. Branching end points are indicated by arrows.

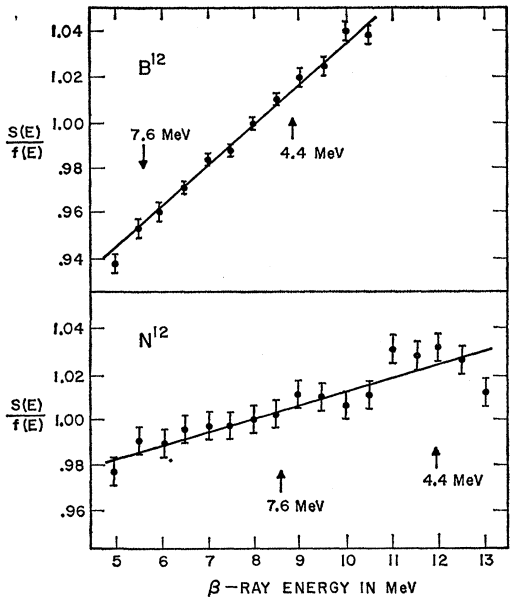

FIG. 11. Plots of the shape factors $S(E,B^{12})/f(E,B^{12})$ and $S(E,N^{12})/f(E,N^{12})$ normalized to unity at 8 MeV. Statistical errors and least-squares fits are shown. Branching end points are indicated by arrows. Slopes are 1.82% per MeV for B^{12} and 0.60% per MeV for N^{12}.

1.3±0.4%, respectively. Thus to construct $S(E,B^{12})$, we first subtract from the observed momentum spectrum the simple ideal Fermi spectra corresponding to these branches. No attempt is made to include possible spectral deviations in the branches themselves, as the error so introduced should be negligible. After this subtraction, the remaining spectrum is divided by the ideal Fermi spectrum corresponding to the ground-state transition to give $S(E,B^{12})$. Finally a correction for inner bremsstrahlung $f(E,B^{12})$, is applied to give the shape factor S/f, which is found, as shown in Fig. 11, to exhibit a linear energy dependence of 1.82±0.09% per MeV. The error (standard deviation) cited derives from the uncertainty in the least-squares fit a of straight line to the data.

For the N^{12} data, additional complications enter since only the branching fraction to the 4.4-MeV state of C^{12}, 2.4±0.2%,[27] has been measured with precision.[29] The branching fraction to the 7.6-MeV state can be estimated to be about 4.0±1.3% from the mirror branching fractions in B^{12} quoted above and the approximation of charge symmetry. The large uncertainties in this branching fraction, introduced by the uncertainty in the mirror branching fraction and by the deviation[27] of the first two branches from the charge

[24] F. Everling, L. A. König, and J. H. E. Mattauch, Nuclear Phys. **15**, 342 (1960).

[25] F. Ajzenberg-Selove, M. L. Bullock, and E. Almqvist, Phys. Rev. **108**, 1284 (1957).

[26] C. W. Cook, W. A. Fowler, C. C. Lauritsen, and T. Lauritsen, Phys. Rev. **107**, 508 (1957).

[27] N. W. Glass, R. W. Peterson, and R. K. Smith, Bull. Am. Phys. Soc. **6**, 49 (1961).

[28] V. Soergel (private communication) reports, however, a larger value for the B^{12} branching ratio to the 7.6-MeV level of C^{12}.

[29] J. F. Vedder, University of California Radiation Laboratory Report UCRL-8324, 1958 (unpublished), analyzed the Fermi plot of N^{12} into linear components using reaction data end points and reports a 3% branch to the 7.6-MeV level which is in agreement with our results, but no uncertainties are quoted. The branching ratio to the 4.4-MeV level is neither in agreement with other experiments (see reference 26) nor in agreement with that expected from the analogous B^{12} branching ratio.

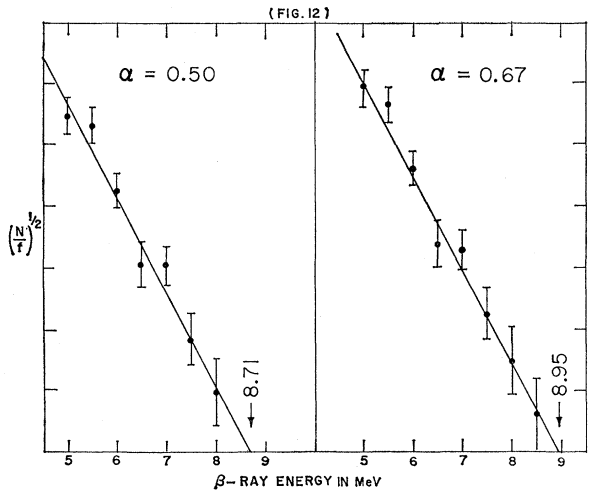

FIG. 12. Fermi plots of the contribution from the 7.6-MeV branch in N^{12} after subtraction of the ground-state transition, assuming the indicated shape factors, and the 4.4-MeV branch using the published branching ratio.[15] The branching ratios indicated by these plots are 3.0 and 3.2% in that order. The end points are given by weighted least-squares fits. Error bars indicate the combined uncertainties of the 4.4-MeV branching ratio and the experimental data. The N^{12}-end point has been taken to be 16.44 MeV in these examples, the end point for the transition to the 7.6-MeV state is then 8.78.

symmetry assumption, then give correspondingly large uncertainties in the form of $S(E,N^{12})$ below 8.5 MeV. For this reason the data has been analyzed to see if a better value for this branching fraction can be determined. This involves decomposing a complex beta-decay spectrum into the separate branches. In principle, the decomposition can be realized by constructing a best fit to the linear portion of the Fermi plot near the end point of the most energetic transition which is then subtracted from the data. This procedure is repeated until either the decomposition is complete or the remaining data after extraction of the n^{th} branch is no longer adequate due to the experimental uncertainties in the data compounded with the uncertainties introduced by each subtraction. For the N^{12} spectrum, many of these uncertainties are avoided by using the branching fraction and end point of the 4.4-MeV branch which are known from independent experiments. Furthermore, the end point of the 7.6-MeV branch is also known from the reaction data, so the problem would actually be overdetermined were it not for the fact that the precise shape of the ground-state transition is not known. In fact, it is just this shape that is to be measured! Advantage of this overdeterminacy is taken by introducing a shape factor of the form $(1+aE)$ into the ground-state spectrum and demanding agreement between the reaction data end point of the 7.6-MeV branch and that found by the subtraction procedure indicated above. In this fashion the quantity a is found to be $0.6\pm0.3\%$ per MeV and the 7.6-MeV branching fraction is $3.0\pm0.4\%$ where the uncertainties are derived from the uncertainties in the various branching end points, in the 4.4-MeV branching fraction, and in the statistical scatter of the data itself. The Fermi plots for two assumed values of the quantity a are shown in Fig. 12. This value of 3.0% for the 7.6-MeV branching fraction, along with the other known branching data, is now used to determine $S(E,N^{12})/f(E,N^{12})$ which is plotted in Fig. 11.

It is readily apparent that the shape factors shown in Fig. 11 differ appreciably from one another; the N^{12} shape factor rises with a slope of $(0.60\pm0.08)\%$ per MeV while the B^{12} rises with a slope of $(1.82\pm0.09)\%$ per MeV. Comparing the two slopes, one finds $(1.22\pm0.13)\%$ per MeV for the experimental value of the factor $A+\delta A$. The uncertainties quoted above are from the statistical scatter of the data alone. Other uncertainties, including that introduced from the branching fraction estimated above, are discussed below. The effect of the uncertain 7.6-MeV branching fraction can be avoided, at the expense of precision, by using the N^{12} data for positron energies greater than 8.0 MeV only. The least-squares fit to this limited portion of the shape factor, which is insensitive to the 7.6-MeV branch, yields an energy dependence of $(0.52\pm0.20)\%$ per MeV and consequently a value of $(1.30\pm0.22)\%$ per MeV for $A+\delta A$.

Errors and Corrections

The sensitivity of the spectrometer to source misalignment has been checked by deliberately placing a Bi^{207} source off axis and also by moving the beam spot 2 mm on the target. No significant effect was observed. Such a misalignment is over ten times what we would reasonably expect during the experiment.

If the upper limit of the HD impurity in the He^3 beam were accepted as being present, then the $A+\delta A$ result would be decreased by 0.02% per MeV.

The uncertainty due to the residual component of the earth's magnetic field is completely negligible at these energies.

In the energy region studied, an error of a constant amount in the background subtraction will lead to a slight curvature of the shape factor but will not essentially change the least-squares fit to the slope. If the background correction is applied assuming that the background has a form $b+cE$ with b and c determined from the high and zero field backgrounds, instead of just averaging the two, then $A+\delta A$ is increased by 0.04% per MeV.

The 1.5-keV uncertainty in the actual end-point energy of the B^{12} transition, given from the reaction data, has negligible influence on the B^{12}-shape factor. On the other hand, the 60-keV uncertainty in the N^{12} end point gives an uncertainty of 0.18% per MeV in the N^{12}-shape factor. If only N^{12} data above 8.0 MeV is used, then this uncertainty is increased to 0.27% per MeV. A 10-keV error in calibration at 13 MeV gives 0.04% per MeV for both B^{12} and N^{12}, but these are in the same di-

rection and give almost no error in the value of $A+\delta A$ which is given by the difference between the two shape factors.

The uncertainty in the branching ratios of B^{12} and N^{12} to the 4.4-MeV state of C^{12} is significant only for the N^{12}-shape factor, where it introduces a 0.04% per MeV uncertainty unless only data above 8.0 MeV is used, whereby this uncertainty is reduced to 0.01% per MeV. The 7.6-MeV branch is unimportant for the B^{12}-shape factor in the energy range considered, but strongly influences the N^{12}-shape factor. The uncertainty in our result for this branching fraction in the N^{12} decay, $(3.0\pm0.4)\%$, introduces an uncertainty of 0.14% per MeV in the slope of the N^{12}-shape factor.

The beta-particle counting efficiency of the anthracene crystal may be energy dependent due to backscattering or, in the N^{12} experiment, annihilation in flight of the decay positrons. In both cases, the beta particle must be lost before sufficient energy has been deposited in the crystal to produce a pulse that will pass the discriminator level. In this experiment such backscattering loss is negligible but the annihilation loss will be significantly greater for the low-energy positrons than for the high-energy positrons and consequently gives the N^{12}-shape factor a spurious slope of approximately $(0.06\pm0.02)\%$ per MeV with the uncertainty due to variations of the discriminator level among the various N^{12} runs. If the beta particle loses a large fraction of its energy via bremsstrahlung, and the bremsstrahlung quanta are not captured, then it will not be counted. Computation indicates that only about 1 in 2×10^4 beta particles are so lost with the experimental arrangement used. Experimentally, the small number of small pulses in the pulse-height distribution testifies to the unimportance of this effect. Annihilation of positrons should also give a contribution to this small-pulse region in the N^{12} experiment, but the statistical accuracy of the data was not sufficient to verify the annihilation correction experimentally.

Finally, we must consider the possibility that beta particles reach the detector by penetrating through the aperture baffle which defines the ring focus and the baffle defining the acceptance solid angle. Such penetration will effectively increase the accepted momentum interval by a factor $1+\alpha E^2$ where α depends upon the geometry and composition of the baffles. This quantity is estimated[30] to be 2.4×10^{-4} $(\text{MeV})^{-2}$ which gives a spurious energy dependence of about 0.38% per MeV for each of the two shape factors. In view of the magnitude of this correction, the absolute shape factors cannot be taken with any confidence. However, the positron penetration is only about 5% greater than the electron penetration so the quantity $A+\delta A$ is increased by only 0.02% per MeV.

The nonlinearity of this correction requires a reexamination of several points, namely the comparison of the B^{12}- and N^{12}-shape factors in slightly different energy regions and the computation of the N^{12} branching fraction to the 7.6-MeV state of C^{12}. It is appropriate here to point out that theoretical estimates[31] of Coulomb, finite nuclear size, and other higher-order corrections predict a curvature of the shape factors of the same magnitude as the slit penetration effect but opposite sign. Taken together, the curvatures then essentially cancel as is suggested experimentally by the B^{12} data. If we suppose that either correction may have been incorrectly estimated by a factor of two, then the existence of these nonlinearities introduces an uncertainty of $\pm0.3\%$ in the 7.6-MeV branching fraction and a net uncertainty of $\pm0.16\%$ per MeV in $A+\delta A$. If N^{12} data above 8.0 MeV is used, the disparity in energy of the data compared is increased but the 7.6-MeV branching fraction has no influence, altogether giving an uncertainty of $\pm0.12\%$ per MeV. If we select only data in the range 8.5 to 10.5 MeV, which is then free both of uncertainties in the 7.6-MeV branching fraction and in nonlinear effects (since we now can compare data at the same energy and the curvatures then cancel in the ratio) we obtain for $A+\delta A$ the value 1.30 ± 0.41.

Summary

The B^{12}-shape factor has an energy dependence of $(1.82\pm0.09)\%$ per MeV while the N^{12}-energy dependence is $(0.60\pm0.08)\%$ per MeV if the value of 3.0% is used for the 7.6-MeV branching fraction, or $0.52\pm0.20\%$ per MeV if only N^{12} data insensitive to this branch is used, giving $(1.22\pm0.13)\%$ and $(1.30\pm0.22)\%$ per MeV, respectively, for $A+\delta A$. The absolute values of the individual shape factors may suffer from important systematic corrections, however these corrections are not expected to appear significantly

TABLE II. Errors (standard deviation).

Source	Error in A+δA (% per MeV)		
Statistics	0.13[a]	0.22[b]	0.41[c]
Calibration	0.00		
B^{12} end-point energy	0.00		
N^{12} end-point energy	0.18[a]	0.27[b]	0.22[c]
4.4-MeV branching of B^{12} decay	0.00		
4.4-MeV branching of N^{12} decay	0.04[a]	0.01[b]	0.02[c]
7.6-MeV branching of B^{12} decay	0.00		
7.6-MeV branching of N^{12} decay	0.14[a]	0.00[b]	0.00[c]
Background correction	0.04		
HD^+ contamination of He^3 beam	0.02		
Backscattering	0.00		
Annihilation	0.02		
Nonlinear corrections	0.16[a]	0.12[b]	0.00[c]
Net Error	0.31[a]	0.37[b]	0.47[c]
Value of A+δA	1.30	1.38	1.38

[a] Error if $(3.0\pm0.4)\%$ used for the 7.6-MeV N^{12} branching fraction.
[b] Error if N^{12} data below 8.5 MeV discounted.
[c] Error if B^{12} and N^{12} data compared in energy region 8.5 −10.5 MeV.

[30] F. Rohrlich and B. C. Carlson, Phys. Rev. **93**, 38 (1954).

[31] M. Morita, Phys. Rev. **113**, 1584 (1959); and J. Bernstein and R. R. Lewis, *ibid.* **112**, 232 (1958).

in the ratio and consequently have small effect on the quantity $A+\delta A$. A value of $(1.30\pm0.41)\%$ per MeV for $A+\delta A$ results if the analysis is further restricted to data in the energy region 8.5 to 10.5 MeV. The uncertainties are only the statistical standard deviations, and therefore we must include the known systematic errors and corrections discussed in the preceding section and listed in Table II. This finally yields for $A+\delta A$ the experimental values $(1.30\pm0.31)\%$, $(1.38\pm0.37)\%$, and $(1.38\pm0.47)\%$ per MeV. These values are all in agreement with the CVC theory prediction of $1.10\pm0.17\%$ per MeV and not in agreement with the Fermi theory estimate of about 0.10% per MeV.

Since the first value has the smallest error and represents the most extensive use of the available data, we select $(1.30\pm0.31)\%$ as being the result of our experiment.

It is interesting to note that the relatively strong energy dependence of the B^{12}-transition matrix element accounts for the failure of Hornyak and Lauritsen[32] to observe a B^{12} branch to the 4.4-MeV state of C^{12}, and in fact gives a Fermi plot that is slightly concave downwards as can be seen in Fig. 10.

As remarked above, there is reason to doubt the absolute shape factors. In this respect it should be noted that the large average shape factor observed (1.18% per MeV) does not seem to be indicated[31] theoretically.

[32] W. F. Hornyak and T. Lauritsen, Phys. Rev. **77**, 160 (1950). For further analysis of their data, see N. W. Tanner, Phil. Mag. **1**, 47 (1956).

ACKNOWLEDGMENTS

The authors are indebted to Professor T. Lauritsen, Professor C. A. Barnes, Professor W. A. Fowler, Professor H. A. Weidenmüller, Professor U. Hauser, and Professor F. Boehm for valuable discussions. Two earlier experiments in this laboratory[33] by H. Hilton and V. Soergel, and H. Hilton and C. Van der Leun provided much of the groundwork which made the present experiment possible. One of us (Mayer-Kuckuk) would like to thank the Deutsches Bundesministerium für Atomkernenergie for financial support and the Kellogg Laboratory for its hospitality.

[33] H. Hilton, Ph.D. thesis, California Institute of Technology, 1960 (unpublished).